Journal of Alloys and Compounds 782 (2019) 852–858

Contents lists available at ScienceDirect

Journal of Alloys and Compounds

journal homepage: http://www.elsevier.com/locate/jalcom

Role of carbon-rings in polycrystalline $GeSb_2Te_4$ phase-change material

Guanjie Wang [a, b], Jian Zhou [a, b], Stephen R. Elliott [c], Zhimei Sun [a, b, *]

[a] School of Materials Science and Engineering, Beihang University, Beijing 100191, China
[b] Center for Integrated Computational Materials Engineering, International Research Institute for Multidisciplinary Science, Beihang University, Beijing 100191, China
[c] Department of Chemistry, University of Cambridge, Cambridge CB2 1EW, United Kingdom

ARTICLE INFO

Article history:
Received 27 October 2018
Received in revised form
15 December 2018
Accepted 17 December 2018
Available online 21 December 2018

Keywords:
Phase-change materials
$GeSb_2Te_4$
Carbon doping
Grain boundary
Ab initio calculations
Ab initio molecular dynamic simulations

ABSTRACT

Carbon (C) is used to increase the overall performance of Ge-Sb-Te (GST) phase-change memory material. Yet the C configuration in polycrystalline GST and its microscopic role is unclear. Using the well-studied $GeSb_2Te_4$ as an example, this work unravels the microscopic C doping role based on *ab initio* calculations. Our results reveal that carbon prefers occupying the interstitials at very low C concentrations, while with a roughly critical C concentration of over 2%, carbon atoms will cluster at the grain boundaries, with very few carbon atoms might exist at the interstitials. With further increasing the C concentrations, C atoms tend to form ring-like configurations in the grain boundaries rather than chain-like configurations. This is due to that the covalent bonds in ring-like configurations are stronger than that in chain-like configurations. Further analysis on the lone-pair electrons and electronic densities of states show that C dopants significantly change the number of lone-pair electrons of surrounding atoms, thus affecting the electronic structure. Finally, the diffusion coefficient of C is estimated to be of the order of 10^{-13} m^2/s at 400 K, indicating the good stability of C dopants in $GeSb_2Te_4$. Our work provides fundamental understanding on the microscopic role of C doping in GST phase-change materials and benefits for improving the properties of the recording materials by controlling the doping concentration.

1. Induction

Ge-Sb-Te (GST) alloys along the Sb_2Te_3-GeTe pseudo-binary compositional tie-line are phase-change materials (PCM) [1–3], and are the most promising candidates for phase-change random-access memory (PCRAM), which is a kind of non-volatile rewritable data-storage memory based on rapid and reversible phase transitions between crystalline and amorphous phases, taking advantage of the difference in resistance properties between the crystalline (low-resistance, SET) and amorphous (high-resistance, RESET) states [4–10]. They also exhibit excellent properties, including high scalability, fast crystallization speed and good cyclability [11,12]. However, to compete with other non-volatile memory devices, the performance of GST-based PCRAM should be further improved; for example, it is an ongoing hot topic to further increase the data-retention ability and reduce the power consumption of PCRAM devices. The data retention and power consumption of a PCRAM device are correlated with the thermal stability, as well as the crystallization temperature, of amorphous GST and the electrical resistivity of crystalline GST, respectively.

To improve the properties of GST, various small radius dopants, such as N [13–15], H [16], O [17–19], and C [20,21], have been explored. Among these dopants, carbon doping has been widely used to enhance the thermal stability of the amorphous state by increasing the degree of disorder and crystallization temperature of the amorphous phase, with a beneficial improvement of the data-retention time at high temperatures [22,23]. On the other hand, phase-change materials doped with C exhibit a large increase of the resistivity of the crystalline state, which lowers the RESET current and hence the power consumption of PCRAM devices [24–26]. Therefore, many efforts have been made in order to understand the role of C dopant, and recent findings show that C strongly modifies the local environment of Ge through the introduction of C–C chains, which can increase the population of tetrahedral Ge atoms to enhance the covalent nature and reduce the number of ABAB-

* Corresponding author. School of Materials Science and Engineering, Beihang University, Beijing 100191, China.
E-mail address: zmsun@buaa.edu.cn (Z. Sun).

https://doi.org/10.1016/j.jallcom.2018.12.228
0925-8388/

type square rings in the amorphous structure [24,27]. In addition, high-resolution transmission electron microscopy (HRTEM) also demonstrates that there is a trend for part of the C atoms to gather at the grain boundaries [28], forming C-rich regions and confining the growth of grains, which improves the performance of GST-based phase-change memory. Although a large number of studies have addressed the influence of C atoms in the amorphous phase [24,29,30], few researchers have focused on the microscopic role of C atoms in polycrystalline configurations. A thorough knowledge of the role of C dopants in the polycrystalline phase is essential for understanding the relationship between properties, the nature of the dopant and the atomic structure of the materials.

In this work, using the well-studied GST composition, $GeSb_2Te_4$ [31], as an example, the microscopic role of C has been investigated by means of *ab initio* calculations. Firstly, the formation energy for doping C at different sites has been calculated to find the most stable configurations. Then, with increasing C concentration, two different configurations formed by C atoms at grain boundaries are discussed. Furthermore, we unravel the effect of C atoms on the electronic properties, along with the corresponding device properties, by investigating the total and partial electronic densities of states (DOS) [32,33]. The electron-localization function (ELF) [34,35] and the effect of C dopants on the lone-pair electrons in the GST system are used to analyze the chemical bonding of C and the reason for its influence on the DOS. Finally, the diffusion coefficient and structural stability of C dopants have also been studied by *ab initio* molecular-dynamics simulations (AIMD).

2. Computational methods

2.1. Density-functional theory (DFT) calculations

Our calculations were carried out within the framework of density-functional theory (DFT), as implemented in the Vienna *ab initio* simulation package (VASP) [36]. Projector-augmented wave (PAW) [37] potentials were used with the generalized-gradient approximation (GGA) [38] and the Perdew-Burke-Ernzerhof (PBE) [39] exchange-correlation functional. The cutoff energy for the plane-wave expansion was 300 eV. The convergence condition was that the energy difference between cycles was less than 1×10^{-5} eV during the self-consistent iterations. The k-point meshes of $4 \times 4 \times 4$ and $6 \times 3 \times 3$ were automatically generated with their origin at the Γ point, and the tetrahedron method with Blchl corrections [40] was used for configurations of Σ3 (111) and Σ5 (100) grain boundaries, respectively. The k-point grid has been tested to be sufficient to obtain converged results. R.I.N.G.S., [41], VESTA [42], and custom-written codes were also utilized for data analysis.

2.2. Construction of models

We chose NaCl-structured cubic $GeSb_2Te_4$ as an initial model, as described in Fig. S1, which contains 12.5% vacancies (Fig. S1(b)) and many interstitial sites (Fig. S1(a)), because the cubic structure of this material is easy to construct, where to obtain a $GeSb_2Te_4$ unit cell, one only needs to remove an atom at the Na site in perfect cubic structure [10,31,43]. The optimized lattice constant for the cubic structure was 6.12, which is in good agreement with experimental values and other theoretical calculations [44,45]. For the purpose of this study, involving the metastable polycrystalline structure, we constructed two grain boundaries with different orientations. One is the most closely packed and stable Σ3 (111) grain boundary, as described in Fig. S1(c), which has 84 atoms and the calculated cohesive energy is −3.610 eV/atom. The other is the Σ5 (100) grain boundary (Fig. S1(d)), which has 70 atoms and its cohesive energy is −3.564 eV/atom, slightly higher than Σ3 (111).

2.3. Ab initio molecular-dynamic simulations

Four grain-boundary models consisting of 6.67% C (90 atoms for Σ3) and 7.89% C (76 atoms for Σ5) were initially constructed, as described above. We used the NVT ensemble and a Nos-Hoover thermostat [46] for AIMD, where a temperature of 400 K was used, which is the same temperature as the 10 years data-retention test for the amorphous structure, the crystalline state also being stable under the same condition. The total simulation time for every process was 72 ps, with a time step of 3 fs. The electron density was sampled for a $2 \times 2 \times 1$ k-point mesh with the pseudopotential energy cut-off set at 300 eV.

3. Results and discussion

The formation energies of the three possible sites of C dopants, with ten different concentrations, are shown in Fig. 1. The cohesive energies of two different configurations formed by C at a grain boundary are also presented in Fig. 2. In order to study the influence of C dopants on the electronic properties, results of DOS for each type of atom with different C concentrations at different sites are shown in Fig. 3. To understand why carbon is more likely to locate at a grain boundary with increasing C concentration, we have extensively investigated the doped system in terms of the chemical bonds and lone-pair electrons by employing the ELF. The results are presented in Figs. 4 and 5. Finally, the results of studying the stability of polycrystalline structures doped with C atoms by AIMD, namely the mean-square displacement (MSD) and partial pair distribution function (PDF), are shown in Figs. 6 and 7.

3.1. Formation energy and cohesive energy of carbon dopants

Where carbon atoms tend to be located in GST (*e.g.* $GeSb_2Te_4$) polycrystalline structures has been one of the most concerning issues when one tries to improve the properties of this phase-change material by doping with C. The C dopant has three possible sites in polycrystalline of $GeSb_2Te_4$, which are a grain boundary, and the interstitial and vacancy sites. Therefore, the formation energies for doping C at these three sites for ten different C-doping concentrations have been calculated using Equation (1) [47]. (The unrelaxed and relaxed structures with concentration of 2.33% are shown in Fig. S2, respectively.)

$$E^f[x] = E_{tot}[x] - E_{tot}[bulk] - n\mu_c \quad (1)$$

where $E_{tot}[x]$ and $E_{tot}[bulk]$ are the total energies of a structure with and without C doping, respectively. n represents the number of carbon atoms, and μ_c is the chemical potential of carbon. In order to compare the formation energy at different concentrations, we divide the total formation energy ($E^f[x]$) by the number of dopant atoms (n), so that the average formation energy of a single dopant atom is obtained. Some useful conclusions can be obtained by the results of Fig. 1. At a low doping concentration of 1.18%, the formation energy for a grain boundary is the highest, while the interstitial site in a grain boundary is more stable. With an increase in the dopant concentration, when the concentration reaches 2.33%, the formation energy for doping C at the grain boundary is the lowest, and with a further increase in C concentration, the carbon atoms tend to cluster at a grain boundary.

As the defective grain boundary of loosely packed atoms may provide several possibilities of how C atoms arrange therein, we have investigated two most possible arrangements for C, *i.e.* chain-like and ring-like configurations (the inset of Fig. 2), for which the calculated cohesive energy are shown in Fig. 2. For each doping

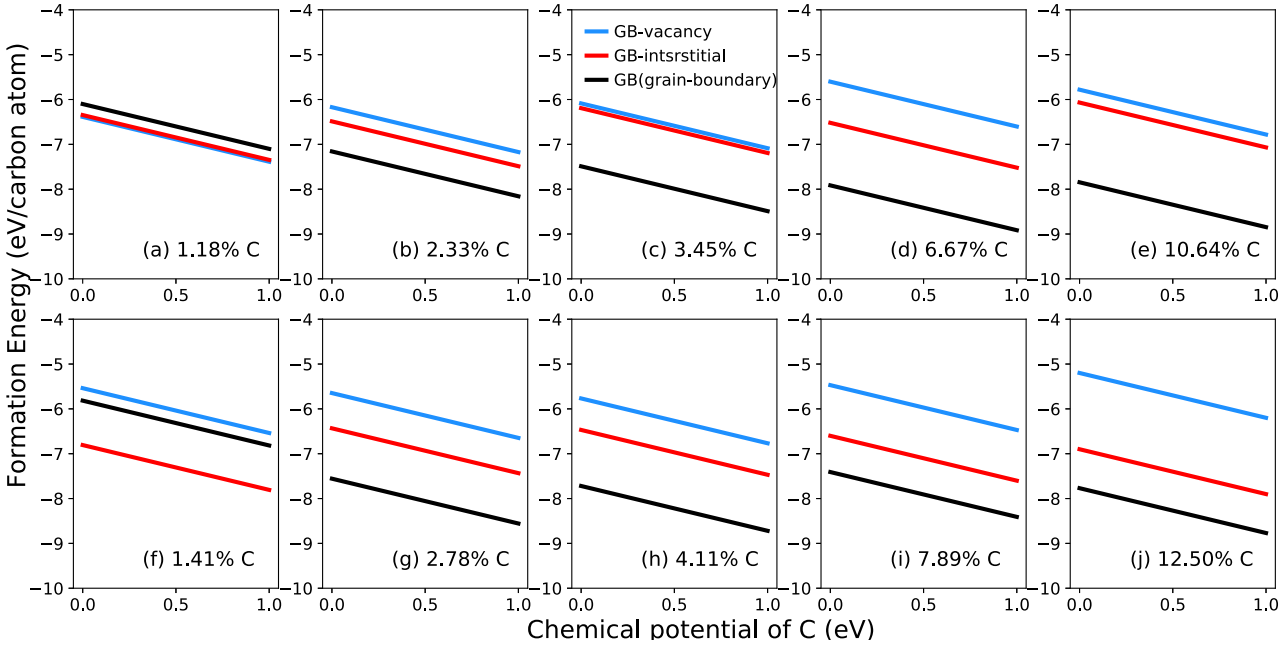

Fig. 1. The formation energy for different dopant concentrations with carbon at different sites, which are grain boundary (black), interstitial (red) and vacancy (blue) sites of a grain boundary. The five graphs (a–e) are for C doped at the Σ3 grain boundary, and the following five (f–j) at the Σ5 grain boundary. (For interpretation of the references to colour in this figure legend, the reader is referred to the Web version of this article.)

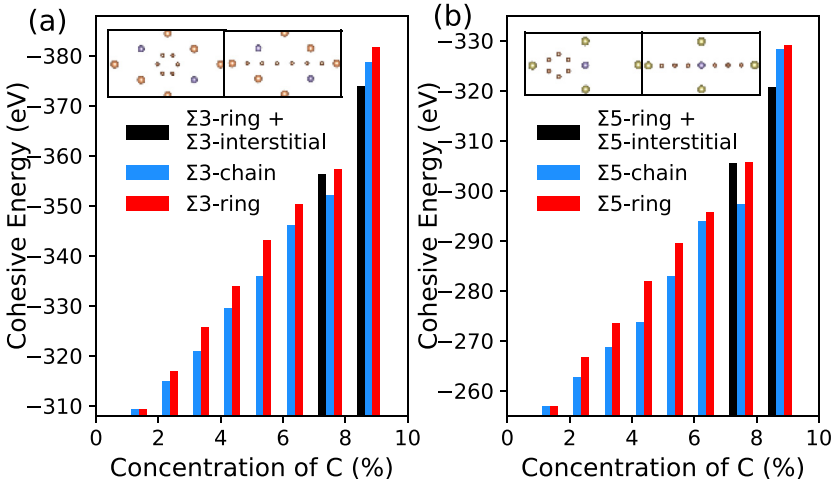

Fig. 2. The cohesive energy of different configurations formed by carbon at: (a) Σ3; and (b) Σ5 grain boundaries. Shown in the insets are the chain-like and ring-like configurations formed by carbon at a grain boundary. Blue, red and black represent dopant configurations of chain-like, ring-like and ring-like plus interstitial carbon, respectively. (For interpretation of the references to colour in this figure legend, the reader is referred to the Web version of this article.)

concentration, the cohesive energy of the ring-like configuration is markedly lower than that of the chain-like configuration, indicating that carbon atoms prefer to form ring-like structures rather than chain-like configurations at the grain boundary.

In addition, considering the lower formation energy for C doped in interstitial positions when the concentration below 2.33%, we thus also considered the situation that some C atoms locate at interstitial sites and others sit at the grain boundary, the calculated results of which are marked as black in Fig. 2. In Fig. 2(a), for the Σ3 grain boundary, the first black part is one interstitial site plus a graphene ring, and its cohesive energy is −356.25 eV, which is comparable to that of the ring-like structure (−357.22 eV) but is lower than that of the chain-like configuration (−352.05 eV). Another situation is four interstitial sites plus a graphene ring, for which the cohesive energy is obviously larger than for the chain- and ring-like configurations. These results demonstrate that only very few carbon dopants may exist in the interstitial sites but the structure will become unstable as the number of C atoms in the interstitial sites increases. The same conclusion is found in Fig. 2(b) for the Σ5 grain boundary. We will discuss in subsection 3.3 why C atoms tend to aggregate at grain boundaries and form ring-like configurations as the dopant concentration increases.

3.2. Electronic properties

Further insight into the effect of C dopants on the electronic properties is shown in Fig. 3. For the grain boundaries of Σ3 and Σ5, it is obvious that there is no band gap for the configurations of

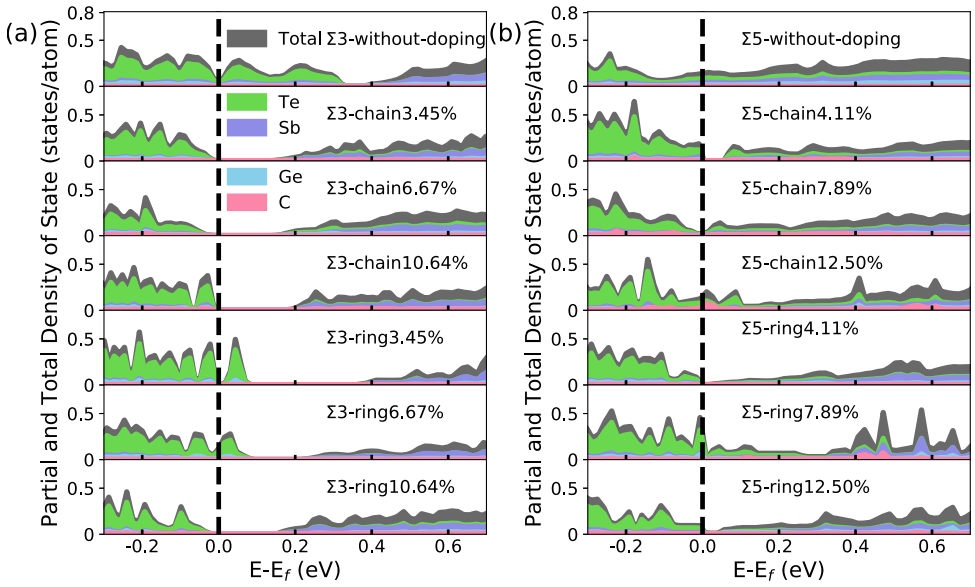

Fig. 3. The partial and total electronic densities of states (DOS) for different configurations formed by carbon with different concentrations at: (a) a Σ3 grain boundary; and: (b) a Σ5 grain boundary. The Fermi energy is set to zero.

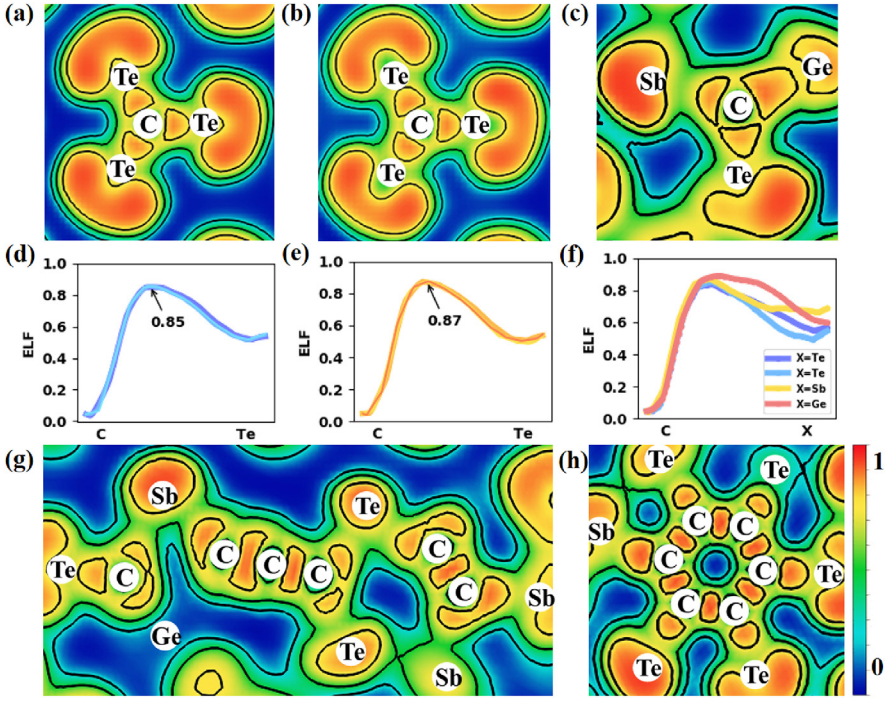

Fig. 4. 2D contour plots of the ELF of C atoms at: (a) vacancy; and (b) interstitial sites of a Σ3 grain boundary; and (c) at the Σ3 grain boundary, respectively, with 2.33% C concentration. And (d)–(e) the corresponding electronic localization function 2D line profiles of the C-X bonds. And (g) chain-like; and (h) ring-like configurations at the Σ3 grain boundary with 6.67% carbon; The ELF scale is from 0 (blue) to 1 (red) and the contour interval is 0.25. Since the two C atoms are not in the same plane in (a–c), we have only focused on one carbon in (a)–(c), and the other one C atom is similar to this one. (For interpretation of the references to colour in this figure legend, the reader is referred to the Web version of this article.)

without C dopants at the above both grain boundaries. With an increase in the doping concentration, the effect of different configurations of C on the electronic structure is shown in Fig. 3(a) and (b), respectively. At the Σ3 grain boundary, as shown in Fig. 3(a), the carbon atoms in chain-like configurations can gradually increase the band gap on increasing the doping concentration from 3.45% to 10.64%, while carbon in the ring-like configurations produces a pseudo-band gap at a concentration of 3.45%, and a large band gap, similar to the chain-like configurations, is produced with an increase in the doping concentration. However, for the case of the Σ5 grain boundary, as seen in Fig. 3(b), carbon atoms in a chain-like configuration produce a small band gap at a concentration of 4.11%, yet as the C concentration increases, the band gap gradually disappears, while C in the ring-like configurations results in no

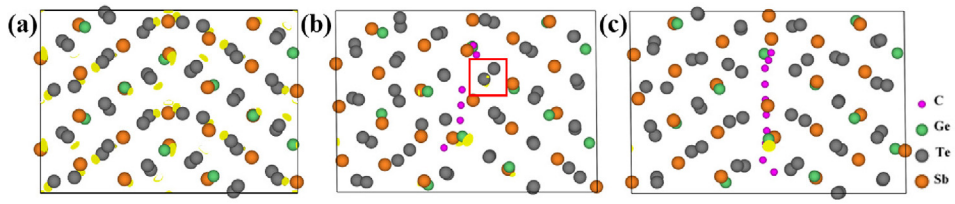

Fig. 5. The 98th percentile ELF isosurface generated to reveal lone-pair electrons for: (a) Σ3 grain boundary without doping, and chain-like configurations with concentrations of: (b) 6.67% and (c) 10.64% carbon at the Σ3 grain boundary. The yellow represent lone-pair electrons and the red boxes mark representative examples of the lone-pair electrons around Te. (For interpretation of the references to colour in this figure legend, the reader is referred to the Web version of this article.)

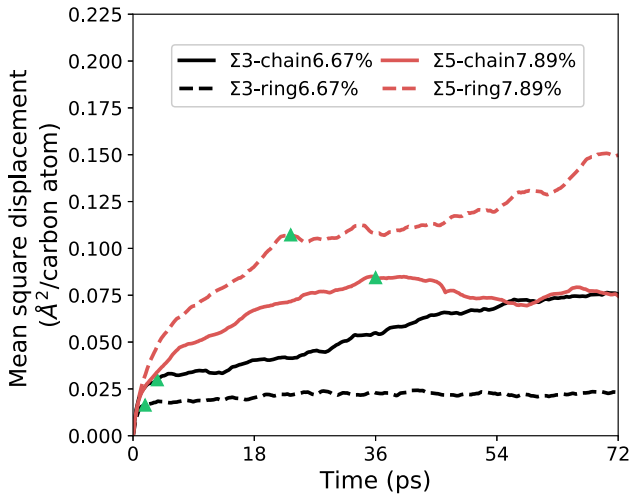

Fig. 6. The mean-square displacement (MSD) of C atoms for chain-like (black solid) and ring-like (black dashed) configurations at the Σ3 grain boundary with 6.67% C, and chain-like (red solid) and ring-like (red dashed) configurations at the Σ5 grain boundary with 7.89% C, respectively. Green triangles divide the line into different regions (D1 and D2) with different diffusivity. (For interpretation of the references to colour in this figure legend, the reader is referred to the Web version of this article.)

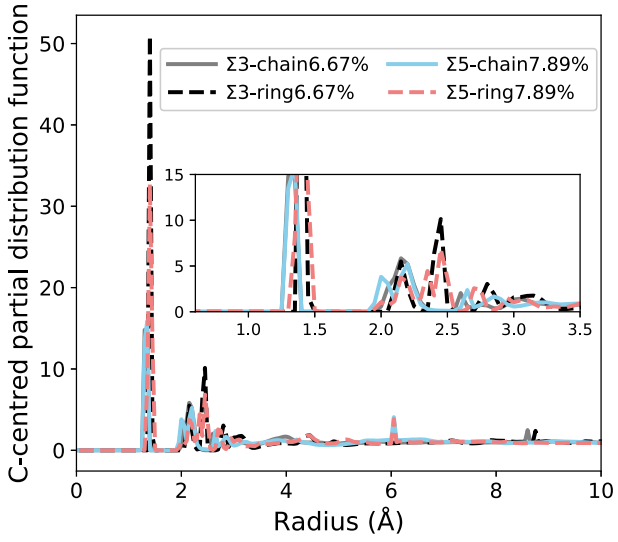

Fig. 7. The partial pair distribution function (PDF) around C for chain-like (grey solid) and ring-like (black dashed) configurations at the Σ3 grain boundary with 6.67% carbon, and chain-like (blue solid) and ring-like (red dashed) configurations at the Σ5 grain boundary with 7.89% carbon. The inset shows a blow-up of the low-PDF region. (For interpretation of the references to colour in this figure legend, the reader is referred to the Web version of this article.)

band gap for all concentrations. In summary, the pristine GST without C doping is metallic because there are some electronic states at the Fermi energy. By C doping with different concentrations, some GST change to semiconductor and the others keep metallic. Obviously, the semiconductor will have increased resistivity compared to metallic. Even for those metallic GST, the electronic states near Fermi energy is smaller than that of pristine one leading to increased resistivity. Furthermore, the segregation of C at grain boundaries will enhance the electron scattering and thus increase the resistivity. The reasons for these results are discussed in detail in the next subsection.

3.3. Chemical-bonding analysis

We have discussed where the C dopants tend to locate and the effect of C doping on the electronic structure of $GeSb_2Te_4$. Further detailed analysis of the mechanism for this behavior will be provided by calculating the ELF and lone-pair electrons, as illustrated in Fig. 4 and 5.

The chemical bond around the carbon atoms with a doping concentration of 2.33% is shown in Fig. 4(a–c). Since the two C atoms are not in the same plane, we have only focused on one carbon, and the other one C atom is similar to this one. It is worth pointing out that the carbon atom can form three equivalent C–Te covalent bonds at the vacancy (Fig. 4(a)) and interstitial site (Fig. 4(b)) of a grain boundary. While in the grain boundary (Fig. 4(c)), there are two C–Te covalent bonds (the two C–Te bonds are not in the same plane, 3D plot can be found in Fig. S3), one C–Sb and one C-Ge covalent bonds which suggest that the four outermost electrons of carbon form exactly four strong covalent bonds at grain boundary, in contrast to the case of three bonds in the vacancy and interstitial of polycrystalline which indicates the existence of non-bonding electrons of C. Fig. 4(d and e) present the corresponding electronic localization function 2D line profiles of the C-X bonds (X represent Sb, Te or Ge), which indicate that the chemical bond of C in interstitials (ELF maximum is 0.87) is slightly stronger than that of C in vacancies (0.85). And these results also reveal that the localization of the electrons is gradually enhanced, and the covalent environment is stronger. Therefore, the doped carbon atoms tend to gather at grain boundaries when the doping concentration is over 2.33%. In addition, to explain why the ring-like configuration is more stable than the chain-like configuration, Fig. 4(g and h) present the ELF of chain-like and ring-like configurations for the Σ3 grain boundary with 6.67% doping concentrations, respectively. Close analysis of the ELF results confirms that C atoms can form strong C–C bonds in chain-like configurations, while in ring-like configurations C will form a π-like bond, which has stronger electronic localization, resulting in the tightly bonded ring-like configuration being more stable than the chain-like configuration. This is similar to that of the Σ5 grain boundary with 7.89% doping concentration (Fig. S4).

To further unravel the mechanism for the effect of C on the

electronic structures, the isosurface corresponding to ELF values at 98% of the local maximum ones are used to identify the position of lone-pair electrons [48], since in electron-rich compounds, such as GST lone-pairs electrons can play an important role in the electronic property and chemical bonding [49]. The ELF isosurface generated at the 98th percentile for different concentrations of C doping at the Σ3 grain boundary are displayed in Fig. 5. As seen in Fig. 5(a) that for the case of Σ3 without doping, the lone-pair electrons are mainly located around Te atoms, with only a few located at around Ge and Sb atoms. These lone-pair electrons will contribute to conducting, which is the origin of the metallic conducting observed in the corresponding DOS in Fig. 3(a). With carbon doping the configuration of lone-pair electrons changes, *i.e.*, the number of lone-pair electrons around Te atoms decreases significantly as seen in Fig. 5(b) and eventually disappears around Te and Sb at a concentration of 10.64% (Fig. 5(c)). This is because that the lone-pair electrons contribute to bonding with the neighboring C atoms, *i.e.*, a strong covalent bond is formed between C and surrounding atoms like Te, Sb and Ge, thus producing a band gap at the Fermi energy. This conclusion can be applied to the case of the Σ5 grain boundary (Fig. S5).

3.4. Ab initio molecular dynamics

Fig. 6 shows the MSD averaged over carbon atoms, for the case of C in chain- and ring-like configurations at Σ3 and Σ5 grain boundaries, respectively. Note that, for the Σ5 ring-like configuration, C atoms move far away from their initial configurations during the simulation. This is because there are many vacancy sites in the grain boundary which provide diffusion channels for C, which results in an obvious inclined distortion (as seen in Fig. S6), while for the case of C forming ring-like configuration at the Σ3 grain-boundary, C atoms just vibrate around a constant MSD value of 0.02. To quantify the atomic dynamics of different configurations, we extracted the diffusion coefficient [50], D, from the atomic displacements as a function of time by linear regression using Tensorflow [51]. For partial atomic diffusion coefficients, we divide each line of the MSD into two sections with different D, separated by green triangles, marked as D1, D2; more detailed values are illustrated in Table 1. For comparison, the diffusion coefficient of carbon in nickel is 2×10^{-4} ^{2}/ps [52]. So, the calculated values of the partial diffusion coefficients indicate that carbon diffuses a very short distance and the systems have reached their thermal-equilibrium states after the second section in the MSD curves. Furthermore, in each section, it is clearly seen that the C atoms in the Σ3-ring-like configuration have the smallest diffusion coefficient, which indicates that the Σ3-ring-like configuration is the first to reach a stable state compared with the other three configurations, and which also suggests that the ring-like configurations formed by carbon at the Σ3 grain boundary are the most stable one. Combined with the results of this subsection, it can be inferred that C dopants tend to concentrate at the stable Σ3 grain boundary rather than at the unstable Σ5 grain boundary.

Further insight into the local structure of near-neighbor atoms of C atoms in different configurations can be obtained by analyzing the PDF around C atoms, the results of which are shown in Fig. 7. It is clear that the sharp first peaks of the partial PDF are located at 1.4 for ring-like configurations, regardless of which grain boundary is doped. Similarly, the peaks of the carbon-centered PDF are located at 1.35 for chain-like configurations. The first peaks of the ring-like configuration are sharp, which means that many equivalent bonds with length of 1.4 were formed between C and surrounding atoms, which is more stable. However, there is a relatively wide peak for the chain structure, indicating that the carbon atoms in the chain-like configurations form many bonds with different bond lengths. That is to say, C is most likely to form a bond of length 1.4 with surrounding atoms, which is very close to that of the C—C bond in graphene, which also may help carbon atoms to form ring-like configurations.

Table 1
The diffusion coefficient, D, (^{2}/ps) of different C configurations in each section of the mean-square displacement profile.

Configurations	D1	D2
Σ3-ring	6.08×10^{-3}	1.09×10^{-5}
Σ3-chain	7.52×10^{-3}	4.05×10^{-4}
Σ5-ring	9.91×10^{-3}	7.02×10^{-4}
Σ5-chain	1.11×10^{-2}	1.35×10^{-3}

4. Conclusions

In summary, by *ab initio* calculations, we revealed that the most stable carbon configurations in polycrystalline GST depend on the doping concentrations. Carbon will randomly occupy the interstitials below a concentration around 2%. While over this critical value carbon will segregate at the grain boundaries to form carbon-rings, which is stable than carbon chains. Further, C dopant significantly changes the number of lone-pair electrons of its neighboring atoms and thus results in different electronic structures of the materials. Finally, the diffusion of C dopant is relatively slow, indicating its good stability in GST.

Acknowledgements

This work is financially supported by the National Key Research and Development Program of China (Grant No. 2017YFB0701700), and the National Natural Science Foundation of China (Grant No. 51872017, 51225205).

Appendix A. Supplementary data

Supplementary data to this article can be found online at https://doi.org/10.1016/j.jallcom.2018.12.228.

References

[1] S.R. Ovshinsky, Reversible electrical switching phenomena in disordered structures, Phys. Rev. Lett. 21 (20) (1968) 1450–1453.
[2] D. Loke, S.R. Elliott, Breaking the speed limits of phase-change memory, Science 336 (6088) (2012) 1566–1569.
[3] M. Wuttig, N. Yamada, Phase-change materials for rewritable data storage, Nat. Mater. 6 (11) (2007) 824–832.
[4] J. Hegeds, S.R. Elliott, Microscopic origin of the fast crystallization ability of ge-sb-te phase-change memory materials, Nat. Mater. 7 (5) (2008) 399.
[5] K. Konstantinou, T.H. Lee, F.C. Mocanu, S.R. Elliott, Origin of radiation tolerance in amorphous ge2sb2te5 phase-change random-access memory material, Proc. Natl. Acad. Sci. U. S. A. 115 (21) (2018) 5353–5358.
[6] Z. Sun, J. Zhou, R. Ahuja, Structure of phase change materials for data storage, Phys. Rev. Lett. 96 (5) (2006), 055507.
[7] T. Siegrist, P. Merkelbach, M. Wuttig, Phase change materials: challenges on the path to a universal storage device, Annu. Rev. Condens. Matter Phys. 3 (3) (2012) 215–237.
[8] Z. Sun, J. Zhou, A. Blomqvist, B. Johansson, R. Ahuja, Formation of large voids in the amorphous phase-change memory ge2sb2te5 alloy, Phys. Rev. Lett. 102 (7) (2009), 075504.
[9] B. Sa, J. Zhou, Z. Song, Z. Sun, R. Ahuja, Pressure-induced topological insulating behavior in the ternary chalcogenide ge2sb2te5, Phys. Rev. B 84 (8) (2011), 085130.
[10] Z. Sun, J. Zhou, R. Ahuja, Unique melting behavior in phase-change materials for rewritable data storage, Phys. Rev. Lett. 98 (5) (2007), 055505.
[11] G.W. Burr, M.J. Breitwisch, M. Franceschini, D. Garetto, K. Gopalakrishnan, B. Jackson, B. Kurdi, C. Lam, L.A. Lastras, A. Padilla, Phase change memory technology, J. Vac. Sci. Technol. B, Nanotechnol. Microelectron.: Mater. Process. Meas. Phenom. 28 (2) (2010) 223–262.
[12] I. Friedrich, V. Weidenhof, W. Njoroge, P. Franz, M. Wuttig, Structural transformations of ge 2 sb 2 te 5 films studied by electrical resistance

measurements, J. Appl. Phys. 87 (9) (2000) 4130–4134.
[13] M.-C. Jung, Y. Lee, H.-D. Kim, M. Kim, H. Shin, K. Kim, S. Song, H. Jeong, C. Ko, M. Han, Ge nitride formation in n-doped amorphous ge2sb2te5, Appl. Phys. Lett. 91 (8) (2007), 083514.
[14] H.K. Kim, S.Y. Lee, D.J. Choi, S. Shin, H.H. Cho, J.S. Roh, Effects of nitrogen doping and working pressure on the crystallization of ge1sb4te7 thin films for pram applications, J. Kor. Phys. Soc. 55 (5) (2009) 1896–1900.
[15] Z. Sun, J. Zhou, H.-J. Shin, A. Blomqvist, R. Ahuja, Stable nitride complex and molecular nitrogen in n doped amorphous ge2sb2te5, Appl. Phys. Lett. 93 (24) (2008), 241908.
[16] S.-W. Kim, W.-S. Lim, T.-W. Kim, H.-Y. Lee, Influence of hydrogenation on the amorphous-to-crystalline phase transition characteristics of ge2sb2te5 and ge8sb2te11 thin films, Jpn. J. Appl. Phys. 47 (7R) (2008) 5337.
[17] K.-B. Song, S.-W. Sohn, J. Kim, K.-A. Kim, K. Cho, Chalcogenide thin-film transistors using oxygenated n-type and p-type phase change materials, Appl. Phys. Lett. 93 (4) (2008), 043514.
[18] L. Zhu, Z. Li, J. Zhou, N. Miao, Z. Sun, Insight into the role of oxygen in the phase-change material gete, J. Mater. Chem. C 5 (14) (2017) 3592–3599.
[19] L. Zhang, N. Miao, J. Zhou, J. Mi, Z. Sun, Insight into the role of w in amorphous gete for phase-change memory, J. Alloys Compd. 738 (2017) 270–276.
[20] B. Sa, Z. Sun, Electron interactions and Dirac fermions in graphene-ge2sb2te5 superlattices, J. Appl. Phys. 115 (23) (2014) 233714.
[21] K.B. Borisenko, Y. Chen, D.J.H. Cockayne, S.A. Song, H.S. Jeong, Understanding atomic structures of amorphous c-doped ge2sb2te5 phase-change memory materials, Acta Mater. 59 (11) (2011) 4335–4342.
[22] G.B. Beneventi, E. Gourvest, A. Fantini, L. Perniola, V. Sousa, S. Maitrejean, J. Bastien, A. Bastard, A. Fargeix, B. Hyot, On carbon doping to improve gete-based phase-change memory data retention at high temperature, in: Memory Workshop (IMW), 2010 IEEE International, IEEE, 2010, pp. 1–4.
[23] G.B. Beneventi, L. Perniola, A. Fantini, D. Blachier, A. Toffoli, E. Gourvest, S. Maitrejean, V. Sousa, C. Jahan, J. Nodin, Carbon-doped gete phase-change memory featuring remarkable reset current reduction, in: Solid-state Device Research Conference (ESSDERC), 2010 Proceedings of the European, IEEE, 2010, pp. 313–316.
[24] G.E. Ghezzi, J.Y. Raty, S. Maitrejean, A. Roule, E. Elkaim, F. Hippert, Effect of carbon doping on the structure of amorphous gete phase change material, Appl. Phys. Lett. 99 (15) (2011) 151906.
[25] Q. Hubert, C. Jahan, A. Toffoli, G. Navarro, S. Chandrashekar, P. Noe, D. Blachier, V. Sousa, L. Perniola, J.-F. Nodin, Lowering the reset current and power consumption of phase-change memories with carbon-doped ge2sb2te5, in: Memory Workshop (IMW), 2012 4th IEEE International, IEEE, 2012, pp. 1–4.
[26] G. Betti Beneventi, L. Perniola, V. Sousa, E. Gourvest, S. Maitrejean, J.C. Bastien, A. Bastard, B. Hyot, A. Fargeix, C. Jahan, J.F. Nodin, A. Persico, A. Fantini, D. Blachier, A. Toffoli, S. Loubriat, A. Roule, S. Lhostis, H. Feldis, G. Reimbold, T. Billon, B. De Salvo, L. Larcher, P. Pavan, D. Bensahel, P. Mazoyer, R. Annunziata, P. Zuliani, F. Boulanger, Carbon-doped gete: a promising material for phase-change memories, Solid State Electron. 65–66 (2011) 197–204.
[27] E. Cho, Y. Youn, S. Han, Enhanced amorphous stability of carbon-doped ge2sb2te5: ab initio investigation, Appl. Phys. Lett. 99 (18) (2011) 183501.
[28] T. Li, L. Wu, X. Ji, Y. Zheng, G. Liu, Z. Song, J. Shi, M. Zhu, S. Song, S. Feng, Carbon doping induced ge local structure change in as-deposited ge2sb2te5 film by exafs and Raman spectrum, AIP Adv. 8 (2) (2018), 025201.
[29] J.-Y. Raty, C. Otjacques, J.-P. Gaspard, C. Bichara, Amorphous structure and electronic properties of the ge1sb2te4 phase change material, Solid State Sci. 12 (2) (2010) 193–198.
[30] K.-C. Chang, R. Zhang, T.-C. Chang, T.-M. Tsai, J.C. Lou, J.-H. Chen, T.-F. Young, M.-C. Chen, Y.-L. Yang, Y.-C. Pan, G.-W. Chang, T.-J. Chu, C.-C. Shih, J.-Y. Chen, C.-H. Pan, Y.-T. Su, Y.-E. Syu, Y.-H. Tai, S.M. Sze, Origin of hopping conduction in graphene-oxide-doped silicon oxide resistance random access memory devices, IEEE Electron. Device Lett. 34 (5) (2013) 677–679.
[31] Z. Sun, J. Zhou, A. Blomqvist, L. Xu, R. Ahuja, Local structure of liquid ge(1)sb(2) te(4) for rewritable data storage use, J. Phys. Condens. Matter 20 (20) (2008), 205102.
[32] T.H. Lee, S.R. Elliott, The relation between chemical bonding and ultrafast crystal growth, Adv. Mater. 29 (24) (2017) 1700814.
[33] Z. Li, N. Miao, J. Zhou, H. Xu, Z. Sun, Reduction of thermal conductivity in yxsb2-xte3 for phase change memory, J. Appl. Phys. 122 (19) (2017), 195107.
[34] A. Savin, R. Nesper, S. Wengert, T.F. Fssler, Elf: the electron localization function, Angew Chem. Int. Ed. Engl. 36 (17) (1997) 1808–1832.
[35] A.D. Becke, K.E. Edgecombe, A simple measure of electron localization in atomic and molecular systems, J. Chem. Phys. 92 (9) (1990) 5397–5403.
[36] G. Kresse, J. Hafner, Ab initio molecular dynamics for open-shell transition metals, Phys. Rev. B 48 (17) (1993) 13115.
[37] B. Pe, Projector augmented-wave method, Phys. Rev. B Condens. Matter 50 (24) (1994) 17953–17979.
[38] J.P. Perdew, K. Burke, M. Ernzerhof, Generalized gradient approximation made simple, Phys. Rev. Lett. 77 (18) (1996) 3865.
[39] J.P. Perdew, Y. Wang, Accurate and simple analytic representation of the electron-gas correlation energy, Phys. Rev. B 45 (23) (2008) 13244.
[40] Bl,P.E. Ouml, O. Jepsen, O.K. Andersen, Improved tetrahedron method for brillouin-zone integrations, Phys. Rev. B 49 (23) (1994) 16223.
[41] S. Le Roux, P. Jund, Ring statistics analysis of topological networks: new approach and application to amorphous ges2 and sio2 systems, Comput. Mater. Sci. 49 (1) (2010) 70–83.
[42] K. Momma, F. Izumi, Vesta 3 for three-dimensional visualization of crystal, volumetric and morphology data, J. Appl. Crystallogr. 44 (6) (2011) 1272–1276.
[43] M. Wuttig, D. Lüsebrink, D. Wamwangi, W. Welnic, M. Gilleßen, R. Dronskowski, The role of vacancies and local distortions in the design of new phase-change materials, Nat. Mater. 6 (2) (2007) 122–128.
[44] Z.L. Mao, H. Chen, A. Jung, The structure and crystallization characteristics of phase change optical disk material ge1sb2te4, J. Appl. Phys. 78 (4) (1995) 2338–2342.
[45] T. Zhang, Z. Song, B. Liu, G. Feng, S. Feng, B. Chen, Effect of structural transformation on the electrical properties for ge1sb2te4 thin film, Thin Solid Films 516 (1) (2007) 42–46.
[46] S.D. Bond, B.J. Leimkuhler, B.B. Laird, The nospoincar method for constant temperature molecular dynamics, J. Comput. Phys. 151 (1) (1999) 114–134.
[47] Z. Li, C. Si, J. Zhou, H. Xu, Z. Sun, Yttrium-doped sb2te3: a promising material for phase-change memory, ACS Appl. Mater. Interfaces 8 (39) (2016) 26126–26134.
[48] G. Gibbs, D. Cox, M. Boisen Jr., R. Downs, N. Ross, The electron localization function: a tool for locating favorable proton docking sites in the silica polymorphs, Phys. Chem. Miner. 30 (5) (2003) 305–316.
[49] J. Zhou, Z. Sun, Y. Pan, Z. Song, R. Ahuja, Vacancy or not: an insight on the intrinsic vacancies in rocksalt-structured gesbte alloys from ab initio calculations, Epl 95 (95) (2011) 27002.
[50] J.-Y. Raty, V. Godlevsky, J.-P. Gaspard, C. Bichara, M. Bionducci, R. Bellissent, R. Colin, J.R. Chelikowsky, P. Ghosez, Local structure of liquid gete via neutron scattering and ab initio simulations, Phys. Rev. B 65 (11) (2002), 115205.
[51] M. Abadi, P. Barham, J. Chen, Z. Chen, A. Davis, J. Dean, M. Devin, S. Ghemawat, G. Irving, M. Isard, Tensorflow: a system for large-scale machine learning, in: OSDI, vol. 16, 2016, pp. 265–283.
[52] J. Lander, H. Kern, A. Beach, Solubility and diffusion coefficient of carbon in nickel: reaction rates of nickel carbon alloys with barium oxide, J. Appl. Phys. 23 (12) (1952) 1305–1309.